

# DiffusionFF: A Diffusion-based Framework for Joint Face Forgery Detection and Fine-Grained Artifact Localization

Siran Peng<sup>1,2\*</sup> Haoyuan Zhang<sup>2,1\*</sup> Li Gao<sup>3</sup> Tianshuo Zhang<sup>2,1</sup>  
 Xiangyu Zhu<sup>1,2</sup> Bao Li<sup>1,2</sup> Weisong Zhao<sup>4,5</sup> Zhen Lei<sup>1,2,6,7†</sup>

<sup>1</sup>MAIS, CASIA <sup>2</sup>SAI, UCAS <sup>3</sup>CMFT <sup>4</sup>IIE, CAS <sup>5</sup>SCS, UCAS <sup>6</sup>CAIR, HKISI, CAS <sup>7</sup>SCSE, FIE, M.U.S.T  
 {pengsiran2023, zhanghaoyuan2023, zhen.lei}@ia.ac.cn

## Abstract

The rapid evolution of deepfake technologies demands robust and reliable face forgery detection algorithms. While determining whether an image has been manipulated remains essential, the ability to precisely localize forgery clues is also important for enhancing model explainability and building user trust. To address this dual challenge, we introduce DiffusionFF, a diffusion-based framework that simultaneously performs face forgery detection and fine-grained artifact localization. Our key idea is to establish a novel encoder–decoder architecture: a pretrained forgery detector serves as a powerful “artifact encoder”, and a denoising diffusion model is repurposed as an “artifact decoder”. Conditioned on multi-scale forgery-related features extracted by the encoder, the decoder progressively synthesizes a detailed artifact localization map. We then fuse this fine-grained localization map with high-level semantic features from the forgery detector, leading to substantial improvements in detection capability. Extensive experiments show that DiffusionFF achieves state-of-the-art (SOTA) performance across multiple benchmarks, underscoring its superior effectiveness and explainability.

## 1. Introduction

The rapid advancement of deepfake technologies [15, 21, 31, 39] has enabled the creation of forged facial content with highly convincing perceptual quality, posing serious threats to information integrity and public trust. This escalating concern underscores the urgent demand for robust and reliable face forgery detection algorithms. Traditionally, research in this area focuses on the binary classification task of determining whether an image has been manipulated. However, there is a growing recognition of the need to precisely localize forgery clues. By pinpointing

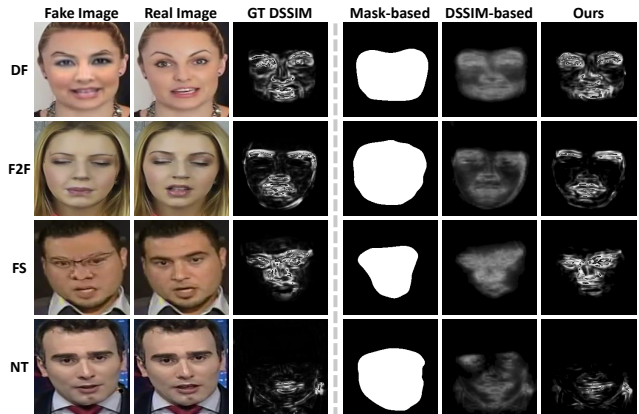


Figure 1. Visual comparison of DiffusionFF with mask-based and existing DSSIM-based artifact localization methods across four manipulation types (DF, F2F, FS, and NT) from the FaceForensics++ (FF++) dataset [37]. The Ground-Truth (GT) DSSIM map is generated by comparing each fake image with its corresponding real image using the algorithm detailed in Section 3.1.1.

the manipulation traces within an image, artifact localization offers clear, human-interpretable evidence that supports the model’s decisions, thereby improving explainability and fostering greater user trust. To simultaneously achieve both objectives, recent studies are increasingly exploring unified frameworks that integrate detection and artifact localization.

However, the precise localization of fine-grained forgery clues remains a significant challenge. Conventional mask-based methods [16, 20, 62] are inherently coarse, highlighting only broad regions of manipulation. To overcome this limitation, several studies have explored using Structural Dissimilarity (DSSIM) maps [50] to guide localization map generation. By directly comparing pixel-level differences between aligned real and fake image pairs, DSSIM maps effectively capture subtle forgery artifacts. Despite this potential, existing DSSIM-based approaches [3, 49] are constrained by their reliance on direct regression frameworks,

\*Equal Contribution.

†Corresponding author.

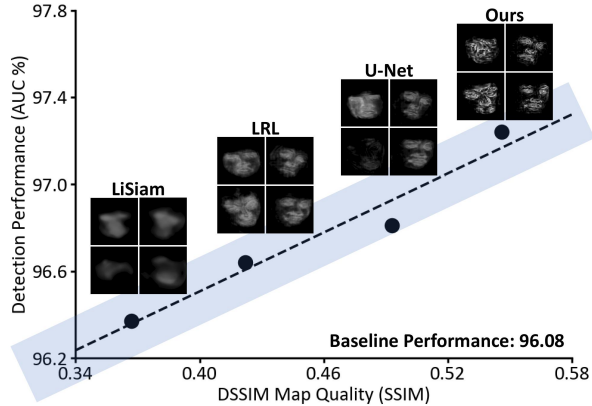


Figure 2. Correlation between the quality of the estimated DSSIM maps and detection performance. We fuse the DSSIM maps estimated by LiSiam [49], LRL [3], U-Net [36], and our DiffusionFF with high-level semantic features from a shared forgery detector to obtain classification results. Integrating estimated DSSIM maps into the detection network consistently improves performance, with higher-quality maps leading to greater performance gains.

which tend to smooth over subtle manipulation traces, resulting in blurry and less informative localization maps. A visual comparison of these methods is presented in Figure 1.

In [49], the estimated DSSIM maps are reintegrated into the network to enhance detection capability. This strategy serves as a key motivation for our work. As shown in Figure 2, our analysis reveals a strong correlation between the quality of these maps and overall detection performance. Specifically, incorporating estimated DSSIM maps into the detection network consistently improves performance, with higher-quality maps leading to greater performance gains.

Considering these factors, we propose DiffusionFF, a novel framework designed to simultaneously tackle the dual challenges of face forgery detection and fine-grained artifact localization. The core innovation of DiffusionFF lies in its rational and intuitive encoder-decoder architecture, where a pretrained forgery detector functions as a powerful “artifact encoder”, and a denoising diffusion model [14] is repurposed as an “artifact decoder”. Conditioned on multi-scale forgery-relevant features extracted by the encoder, the decoder progressively estimates a detailed DSSIM map, which precisely localizes fine-grained forgery clues. This estimated DSSIM map is subsequently fused with high-level semantic features from the forgery detector, leading to substantial improvements in detection performance. In conclusion, the contributions of this paper are as follows:

- We establish a novel encoder-decoder architecture that leverages a pre-trained forgery detector as an “artifact encoder” and repurposes a denoising diffusion model as an “artifact decoder”. Conditioned on multi-scale forgery-related features from the encoder, the decoder progres-

sively synthesizes a fine-grained artifact localization map.

- We integrate the generated localization map with high-level semantic features from the forgery detector, resulting in significant improvements in detection capability.
- DiffusionFF achieves state-of-the-art (SOTA) detection performance and surpasses existing artifact localization methods in revealing manipulation traces, demonstrating its superior effectiveness, reliability, and explainability.

## 2. Related Works & Motivation

### 2.1. Face Forgery Detection

#### 2.1.1. Detection-only Methods

Detection-only methods for face forgery detection primarily focus on achieving high accuracy, typically only providing a binary classification outcome. Existing studies, based on their underlying strategies, can be grouped into four main categories [32]: spatial-domain, time-domain, frequency-domain, and data-driven approaches. Spatial-domain methods detect forgeries by analyzing image-level artifacts such as color mismatches [12], unnatural saturation [28], and visual anomalies [5, 55, 61]. Time-domain techniques model temporal dynamics across video frames to capture inter-frame inconsistencies [54, 58]. Frequency-domain methods apply algorithms like the Fast Fourier Transform (FFT) [42], Discrete Cosine Transform (DCT) [34], and Discrete Wavelet Transform (DWT) [18, 23, 33] to expose subtle manipulation traces that are often imperceptible in the spatial or time domains. Lastly, data-driven approaches boost detection performance by leveraging advanced network architectures and optimized training strategies [17, 51, 52, 63].

#### 2.1.2. Joint Detection and Localization Methods

In addition to detection-only approaches, some studies have developed unified frameworks capable of simultaneously performing face forgery detection and artifact localization. These methods can be broadly classified into two types: mask-based and DSSIM-based approaches. Mask-based methods treat artifact localization as a segmentation task, generating binary masks that indicate forged regions. These methods primarily exploit semantic features, analyze noise patterns, or leverage meta-learning techniques to improve segmentation precision [16, 20, 62]. In contrast, DSSIM-based approaches aim to produce fine-grained, pixel-level localization maps that reveal subtle traces of manipulation. To enhance localization quality, these approaches have explored attention mechanisms [3] or Siamese network architectures [49]. Unlike coarse binary masks, DSSIM maps offer a more precise and detailed representation of forgery artifacts. However, existing DSSIM-based methods rely on direct regression frameworks, leading to blurry and overly smoothed outputs. This limitation prevents these methods from fully harnessing the rich potential of DSSIM maps.

## 2.2. Diffusion Models in Forgery Detection

In recent years, diffusion models [14] have emerged as a powerful class of generative tools, which iteratively transform noise into high-fidelity images by learning the underlying data distribution through a denoising process. In image forgery detection, DiffForensics [57] leverages diffusion models as robust image priors to detect manipulations and create binary masks highlighting forged regions. In the specific domain of face forgery detection, Diffusion-Fake [4] employs a Latent Diffusion Model (LDM) [35] to reconstruct both the source and target identities from a single deepfake image. However, despite these advancements, the potential of diffusion models to synthesize fine-grained artifact localization maps remains largely unexplored.

## 2.3. Motivation

Recent studies are increasingly exploring unified frameworks that jointly address face forgery detection and artifact localization. Conventional mask-based methods provide only coarse localization of forged regions. On the other hand, while DSSIM maps can capture fine-grained manipulation traces, existing DSSIM-based approaches often produce blurry outputs due to their reliance on direct regression frameworks. To overcome these limitations and fully exploit the potential of DSSIM maps, we establish a novel encoder-decoder architecture that leverages a pre-trained forgery detector as an ‘‘artifact encoder’’ and repropose a diffusion model as an ‘‘artifact decoder’’. Conditioned on forgery-relevant features from the encoder, the decoder progressively estimates a detailed DSSIM map, enabling precise localization of fine-grained artifacts. Motivated by our analysis in Figure 2, we fuse the estimated DSSIM map with high-level semantic features from the detector, leading to substantial improvements in detection performance.

## 3. Methodology

### 3.1. Preliminaries

#### 3.1.1. GT DSSIM Map Formulation

To generate Ground-Truth (GT) DSSIM maps for supervising the training of denoising diffusion models and for evaluation purposes, we first extract frames and crop faces from both the original facial video and its manipulated counterparts, ensuring consistent settings across different video types. This process yields a set of fully aligned image pairs. For each image pair, we compute the DSSIM map by sliding a local square window across the two images and calculating the DSSIM value at each pixel location  $(i, j)$ . The computation can be mathematically expressed as follows:

$$\begin{aligned} \text{DSSIM}(i, j) &= 1 - \text{SSIM}(x, y), \\ \text{SSIM}(x, y) &= \frac{(2\mu_x\mu_y + C_1)(2\sigma_{xy} + C_2)}{(\mu_x^2 + \mu_y^2 + C_1)(\sigma_x^2 + \sigma_y^2 + C_2)}. \end{aligned} \quad (1)$$

Here,  $\text{DSSIM}(i, j)$  is the DSSIM value at the pixel position  $(i, j)$ . The variables  $x$  and  $y$  represent the local square windows centered at  $(i, j)$  in the original and manipulated images.  $\mu_x$  and  $\mu_y$  are the mean intensities of windows  $x$  and  $y$ , while  $\sigma_x$  and  $\sigma_y$  denote the variances of the corresponding windows.  $\sigma_{xy}$  represents the covariance between the two windows. The constants  $C_1$  and  $C_2$  are small values added to ensure numerical stability. Notably, DSSIM maps are computed only for fake images, while real images are assigned pure black maps to represent zero dissimilarity.

#### 3.1.2. Diffusion Model Training

We train our generative model following the Denoising Diffusion Probabilistic Model (DDPM) framework [14], which involves two primary processes: a forward diffusion process and a reverse denoising process. The forward process is a fixed Markov chain that progressively adds Gaussian noise to a clean image  $x_0$  over  $T$  timesteps. This process has a key property that a noisy image  $x_t$  at any timestep  $t$  can be directly sampled from the original image  $x_0$  as follows:

$$x_t = \sqrt{\bar{\alpha}_t}x_0 + \sqrt{1 - \bar{\alpha}_t}\epsilon, \quad (2)$$

where  $\epsilon \sim \mathcal{N}(0, \mathbf{I})$  is a random noise sample. The noise level is dictated by a predefined variance schedule  $\{\beta_t\}_{t=1}^T$ . From this, we define  $\alpha_t = 1 - \beta_t$  and the cumulative product  $\bar{\alpha}_t = \prod_{i=1}^t \alpha_i$ . The reverse process aims to train a denoising network  $\epsilon_\theta(x_t, t)$  that predicts the noise  $\epsilon$  added to the noisy image  $x_t$ . The training objective is to minimize the Mean Squared Error (MSE) between the predicted noise and the true noise, which can be expressed as follows:

$$\mathcal{L}_{\text{MSE}} = \mathbb{E}_{x_0, \epsilon, t} \left[ \|\epsilon - \epsilon_\theta(x_t, t)\|_2^2 \right]. \quad (3)$$

#### 3.1.3. Diffusion Model Inference

During inference, the trained generative model reverses the forward diffusion process to reconstruct clean images from noisy inputs. Starting from a fully noisy image  $x_T$ , the model iteratively applies the reverse denoising process to refine it, eventually recovering the clean image  $x_0$ . At each timestep  $t$ , the denoising network  $\epsilon_\theta(x_t, t)$  predicts the noise  $\epsilon$  added to the image. The model then removes the predicted noise from the current noisy image  $x_t$  to produce a less noisy version  $x_{t-1}$ , using the following update rule:

$$x_{t-1} = \frac{1}{\sqrt{\alpha_t}} \left( x_t - \frac{\beta_t}{\sqrt{1 - \bar{\alpha}_t}} \epsilon_\theta(x_t, t) \right) + \sqrt{\frac{1 - \bar{\alpha}_{t-1}}{1 - \bar{\alpha}_t}} \beta_t \cdot z, \quad (4)$$

where  $z \sim \mathcal{N}(0, \mathbf{I})$  is a random noise sample when  $t > 1$ . This process is repeated for each  $t$  from  $T$  down to 1, gradually refining the image until a clean sample is generated.

## 3.2. DiffusionFF

### 3.2.1. Overall Architecture

The proposed DiffusionFF framework simultaneously performs face forgery detection and fine-grained artifact local-

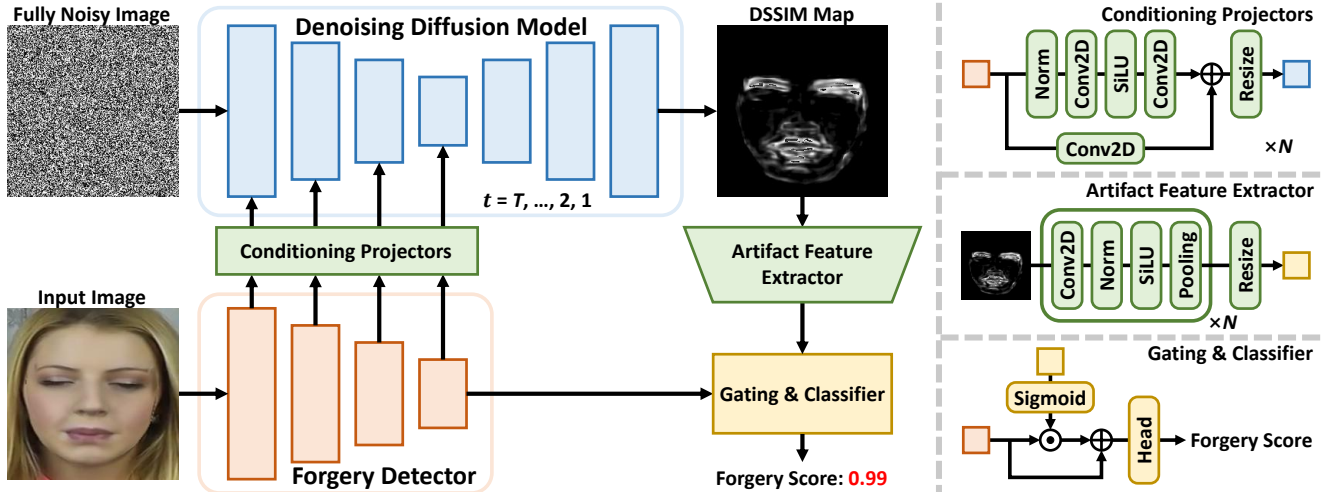


Figure 3. Overview of the DiffusionFF framework. Given an input facial image, DiffusionFF simultaneously predicts a forgery score and estimates a DSSIM map that precisely localizes fine-grained facial forgery clues.  $N$  denotes the number of stages in the forgery detector.

ization, as illustrated in Figure 3. Given an input facial image, a pretrained forgery detector first extracts multi-scale features that encode forgery-related information. These features are then injected into the diffusion model via conditioning projectors to guide the generative process. Starting from random noise, the diffusion model progressively estimates a detailed DSSIM map that precisely localizes fine-grained forgery clues. An artifact feature extractor subsequently extracts informative features from the estimated DSSIM map. Finally, these artifact-aware features are integrated with high-level features from the detector through a gating mechanism to produce the classification outcome.

### 3.2.2. Conditional DSSIM Map Estimation via Diffusion

In previous studies, direct regression frameworks have been used to estimate DSSIM maps. However, such approaches often oversmooth subtle manipulation traces, resulting in blurry and less informative artifact localization. In contrast, diffusion models inherently support iterative refinement, allowing them to progressively enhance outputs and better capture fine-grained inconsistencies. Motivated by this advantage, we leverage a denoising diffusion model to estimate detailed DSSIM maps. To guide this generative process, we employ a pretrained forgery detector, which functions as a powerful “artifact encoder”, to extract multi-scale features from the input facial image. Conditioned on these forgery-relevant features, the diffusion model is thus repurposed as an “artifact decoder”, progressively synthesizing a fine-grained artifact localization map. Notably, we observe that jointly training the detector and diffusion model from scratch leads to training collapse, underscoring the importance of incorporating pre-learned forgery knowledge into the generation pipeline. To achieve this effective knowl-

edge transfer, we design a set of conditioning projectors. These modules bridge the gap between the two models by aligning the spatial and channel dimensions of the detector’s multi-scale features with the U-Net backbone [36] of the diffusion model. Once aligned, the forgery-related features are injected into the corresponding U-Net encoder stages, allowing the denoising diffusion model to fully exploit the detector’s guidance and estimate detailed DSSIM maps.

### 3.2.3. Feature Fusion and Classification

Figure 2 demonstrates that integrating the estimated DSSIM maps into the detection network consistently improves performance. Therefore, we leverage the estimated high-fidelity DSSIM map to guide the final classification. Specifically, an artifact feature extractor first encodes the DSSIM map into artifact-aware features that capture subtle manipulation traces. These features are spatially and channel-wise aligned with the high-level semantic features from the final stage of the pretrained forgery detector. The two complementary feature sets are then fused via a gating mechanism, allowing the model to selectively emphasize manipulation-relevant regions. Finally, a classifier head produces the prediction. The overall process can be expressed as follows:

$$\text{Score} = \mathcal{H}(\sigma(\mathcal{E}(M_{DSSIM})) \odot F_{det} + F_{det}), \quad (5)$$

where  $M_{DSSIM}$  is the estimated DSSIM map, and  $F_{det}$  represents the detector’s high-level features.  $\mathcal{E}$  denotes the artifact feature extractor,  $\sigma$  is the Sigmoid activation,  $\odot$  represents the Hardamard product, and  $\mathcal{H}$  is the classifier head.

### 3.2.4. Training Strategy

Given the significant differences between DSSIM map estimation and binary classification, jointly optimizing them

Table 1. Cross-dataset face forgery detection performance on the CDF2, DFDC, DFDCP, and FFIW benchmarks. Methods marked with \* are reproduced, while results for others are directly cited from the original papers. For each dataset, the best result is highlighted in **bold** and the second-best is underlined. Methods above the horizontal divider are detection-only, while those below are joint detection and localization approaches. Notably, the proposed DiffusionFF framework consistently achieves SOTA performance across all datasets.

Method	Venue	Localization		Test Set AUC (%) $\uparrow$			
		Mask	DSSIM	CDF2	DFDC	DFDCP	FFIW
DCL [41]	AAAI 2022	$\times$	$\times$	82.30	-	76.71	71.14
SBI [38]	CVPR 2022	$\times$	$\times$	93.18	72.42	86.15	84.83
F <sup>2</sup> Trans [29]	TIFS 2023	$\times$	$\times$	89.87	-	76.15	-
SeeABLE [22]	ICCV 2023	$\times$	$\times$	87.30	75.90	86.30	-
LAA-Net [30]	CVPR 2024	$\times$	$\times$	95.40	-	86.94	-
RAE [46]	ECCV 2024	$\times$	$\times$	95.50	80.20	89.50	-
FreqBlender [64]	NeurIPS 2024	$\times$	$\times$	94.59	74.59	87.56	86.14
UDD [10]	AAAI 2025	$\times$	$\times$	93.10	81.20	88.10	-
DFD-FCG [11]	CVPR 2025	$\times$	$\times$	95.00	81.81	-	-
Effort* [53]	ICML 2025	$\times$	$\times$	<u>95.73</u>	<u>84.78</u>	90.42	<u>88.53</u>
LRL* [3]	AAAI 2021	$\times$	$\checkmark$	91.70	76.66	81.18	82.00
PCL+I2G [63]	ICCV 2021	$\checkmark$	$\times$	90.03	67.52	74.37	-
LiSiam* [49]	TIFS 2022	$\times$	$\checkmark$	90.36	72.59	82.06	76.52
AUNet [1]	CVPR 2023	$\checkmark$	$\times$	92.77	73.82	86.16	81.45
Delocate [16]	IJCAI 2024	$\checkmark$	$\times$	91.30	-	84.00	-
KFD [56]	ICML 2025	$\checkmark$	$\times$	94.71	79.12	<u>91.81</u>	-
DiffusionFF (Ours)	-	$\times$	$\checkmark$	<b>97.24</b>	<b>85.05</b>	<b>92.56</b>	<b>88.56</b>

often leads to suboptimal performance for both. To address this challenge, we propose a two-stage training strategy that fully decouples the two tasks at the training level, enabling dedicated and specialized optimization for each. In the first stage, we freeze the pretrained forgery detector and focus on training the conditioning projectors and the denoising diffusion model. This stage is guided by the loss function defined in Equation 3, ensuring the model is effectively optimized for DSSIM map estimation. In the second stage, we freeze the forgery detector, conditioning projectors, and diffusion model, and instead optimize the artifact feature extractor alongside the classifier. This stage employs the standard Cross-Entropy (CE) loss to enhance classification performance. Our two-stage training strategy fully leverages the capabilities of each network component, ultimately maximizing the effectiveness of the DiffusionFF framework.

## 4. Experiments

### 4.1. Setup

#### 4.1.1. Datasets

We perform model training and intra-dataset evaluation on the widely used FaceForensics++ (FF++) dataset [37], which contains 1,000 real facial videos and 4,000 fake ones

generated by four manipulation techniques: DeepFakes (DF), Face2Face (F2F) [44], FaceSwap (FS), and Neural-Textures (NT) [45]. For cross-dataset evaluation, we select four popular benchmarks: Celeb-DeepFake-v2 (CDF2) [24], which applies advanced deepfake generation methods to YouTube celebrity videos; the DeepFake Detection Challenge (DFDC) [8] and its Preview version (DFDCP) [7], which contain videos with various perturbations such as compression, downsampling, and noise; and FFIW-10K (FFIW) [65], which incorporates multi-person scenarios.

#### 4.1.2. Baselines

We compare our approach with sixteen SOTA baselines for face forgery detection, including ten detection-only methods: DCL [41], SBI [38], F<sup>2</sup>Trans [29], SeeABLE [22], LAA-Net [30], RAE [46], FreqBlender [64], UDD [10], DFD-FCG [11], and Effort [53]; and six joint detection and localization methods: LRL [3], PCL+I2G [63], LiSiam [49], AUNet [1], Delocate [16], and KFD [56]. These baselines cover diverse technical paradigms, from traditional convolutions to SOTA Large Language Models (LLMs).

#### 4.1.3. Evaluation Metrics

We evaluate detection performance using the Area Under the Receiver Operating Characteristic Curve (AUC), a

Table 2. Cross-dataset DSSIM map estimation performance. Note that the DFDC and DFDCP datasets lack GT DSSIM maps because their real and fake video pairs are not spatially aligned.

Dataset	Method	Evaluation Metrics			
		PSNR $\uparrow$	SSIM $\uparrow$	LPIPS $\downarrow$	FID $\downarrow$
CDF2	LiSiam [49]	21.985	0.367	0.464	256.201
	LRL [3]	20.801	0.422	0.455	258.674
	DiffusionFF	<b>30.697</b>	<b>0.546</b>	<b>0.376</b>	<b>98.982</b>
FFIW	LiSiam [49]	23.689	0.421	0.446	284.271
	LRL [3]	23.999	0.460	0.409	248.781
	DiffusionFF	<b>32.828</b>	<b>0.529</b>	<b>0.394</b>	<b>191.798</b>

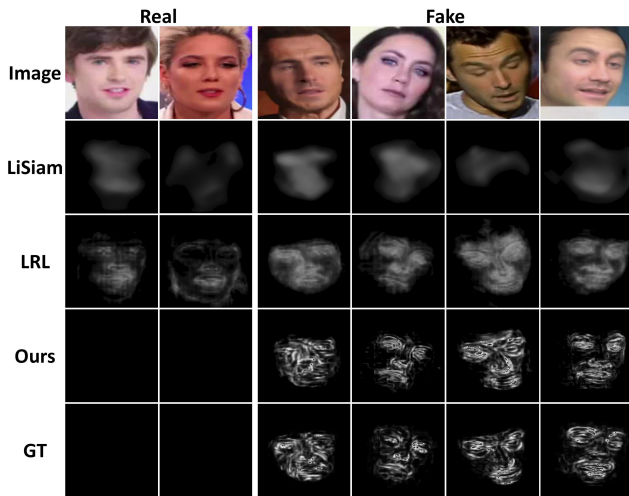


Figure 4. Qualitative DSSIM map estimation results on CDF2. DiffusionFF demonstrates strong generalization ability by producing more precise and fine-grained artifact localization results.

widely adopted metric for face forgery detection. Video-level results are reported by averaging frame-level predictions across each video. To assess the quality of the estimated DSSIM maps, we employ four standard metrics for evaluating image reconstruction and generation: Peak Signal-to-Noise Ratio (PSNR), Structural Similarity (SSIM) [50], Learned Perceptual Image Patch Similarity (LPIPS) [60], and Fréchet Inception Distance (FID) [13].

#### 4.1.4. Implementation Details

For forgery detection, we adopt the preprocessing techniques, data augmentation strategies, and testing pipeline developed by SBI [38]. For artifact localization, we produce GT DSSIM maps on the FF++, CDF2, and FFIW datasets using the procedure outlined in Section 3.1.1. We employ a ConvNeXt-B network [26] pretrained on the FF++ dataset as the forgery detector, which consists of four hierarchical stages. For the denoising diffusion model, we use a U-Net

Table 3. Intra-dataset face forgery detection performance on the FF++ dataset. The proposed DiffusionFF framework yields the best overall results compared to existing SOTA approaches.

Method	Test Set AUC (%) $\uparrow$				
	DF	F2F	FS	NT	FF++
LRL [3]	<b>100</b>	<b>100</b>	99.95	99.59	99.88
PCL+I2G [63]	<b>100</b>	99.57	<b>100</b>	99.58	99.79
LiSiam [49]	<b>100</b>	99.99	99.99	99.46	99.86
AUNet [1]	<b>100</b>	99.86	99.98	99.71	99.89
RAE [46]	99.60	99.10	99.20	97.60	98.90
DiffusionFF	<b>100</b>	<b>100</b>	99.90	<b>99.86</b>	<b>99.94</b>

Table 4. Intra-dataset DSSIM map estimation performance on the FF++ dataset. Our method demonstrates superior performance compared to existing DSSIM-based localization approaches, with particularly significant improvement observed in the FID metric.

Method	Evaluation Metrics			
	PSNR $\uparrow$	SSIM $\uparrow$	LPIPS $\downarrow$	FID $\downarrow$
LiSiam [49]	20.753	0.408	0.426	292.149
LRL [3]	23.608	0.595	0.326	241.625
DiffusionFF	<b>26.376</b>	<b>0.718</b>	<b>0.198</b>	<b>43.093</b>

architecture [36] enhanced with a timestep encoder. Our two-stage training strategy is configured as follows. In the first stage, we train the conditioning projectors and the diffusion model for 100 epochs using the AdamW optimizer [27], with a batch size of 96 and an initial learning rate of  $1 \times 10^{-4}$ , which follows a cosine decay schedule. The total number of diffusion steps is set to  $T = 50$ . In the second stage, the artifact feature extractor and the classifier are trained for 5 epochs using AdamW, with a batch size of 128 and a fixed learning rate of  $5 \times 10^{-5}$ . All experiments are implemented in the PyTorch framework and executed on a cluster of eight NVIDIA RTX 3090 GPUs. For additional details, please kindly refer to the supplementary material.

## 4.2. Performance

### 4.2.1. Cross-Dataset Evaluation

Cross-dataset evaluation is a crucial protocol for assessing the generalization ability of face forgery detection models on previously unseen data. As shown in Table 1, we compare our method against recent SOTA approaches for face forgery detection. The proposed DiffusionFF framework outperforms all competing models, achieving the highest AUC scores across all unseen datasets, demonstrating its exceptional generalization capability. For artifact localization, we conduct both quantitative and qualitative comparisons with existing DSSIM-based techniques. The results

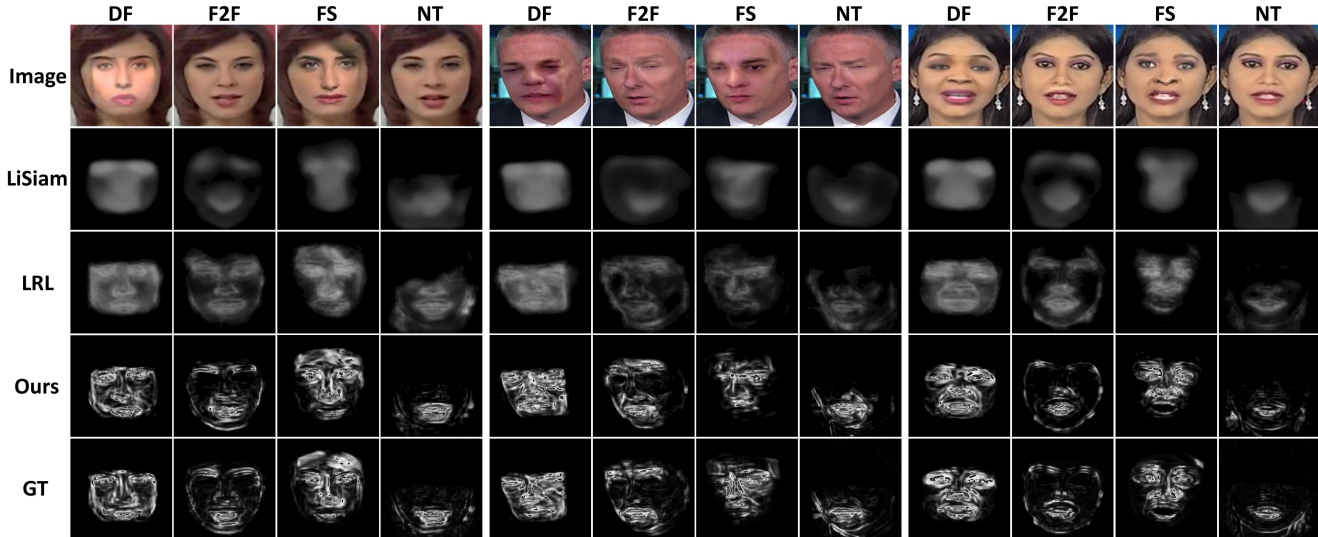


Figure 5. Qualitative DSSIM map estimation results on the FF++ dataset. Our method achieves the most visually faithful outcomes.

Table 5. Ablation study on the diffusion model. Our method produces the highest-quality DSSIM maps, validating the effectiveness of our design choices. “Cond.” is short for conditioning.

Method	Evaluation Metrics			
	PSNR $\uparrow$	SSIM $\uparrow$	LPIPS $\downarrow$	FID $\downarrow$
Direct Regression	24.341	0.584	0.252	172.213
Latent-Space Diffusion	24.228	0.680	0.217	56.384
Final-Stage Cond.	26.154	0.711	0.204	43.812
Decoder Cond.	26.253	0.716	0.202	46.329
The Proposed	<b>26.376</b>	<b>0.718</b>	<b>0.198</b>	<b>43.093</b>

in Table 2 and Figure 4 demonstrate the superior effectiveness of DiffusionFF in producing high-quality localization maps. This remarkable performance can be attributed to the novel application of diffusion models to estimate DSSIM maps, which enables the precise localization of fine-grained forgery clues and ultimately enhances detection capability.

#### 4.2.2. Intra-Dataset Evaluation

In Table 3, we compare the intra-dataset detection performance of DiffusionFF with that of existing approaches, highlighting the superior discriminative power of our method. Furthermore, the quantitative results in Table 4 and qualitative outcomes in Figure 5 validate the efficacy of DiffusionFF in synthesizing high-quality localization maps.

### 4.3. Model Analysis

In this section, we present a comprehensive analysis of the DiffusionFF framework, including ablation studies on the diffusion model and fusion module, as well as evaluations

Table 6. Ablation study on the fusion module. The selected gating mechanism surpasses alternative fusion strategies in face forgery detection, confirming the soundness of our design choice.

Method	Test Set AUC (%) $\uparrow$				Avg.
	CDF2	DFDC	DFDCP	FFIW	
Addition	95.79	84.68	91.56	88.38	90.10
Hadamard Product	96.46	84.53	91.37	88.40	90.19
Concatenation	96.66	85.00	91.87	<b>89.01</b>	90.64
Cross-Attention	97.19	84.91	92.26	88.46	90.71
Gating Mechanism	<b>97.24</b>	<b>85.05</b>	<b>92.56</b>	88.56	<b>90.85</b>

of model generality and robustness. Additional ablation experiments, covering training and inference settings of the diffusion model, denoising seeds, and the two-stage training pipeline, are all detailed in the supplementary material.

#### 4.3.1. Ablation Study on the Diffusion Model

We conduct a series of ablation experiments to evaluate the key design choices in our denoising diffusion model for fine-grained artifact localization. Specifically, our experiments investigate: (1) the effectiveness of iterative generation compared to direct regression; (2) the impact of utilizing diffusion models at the pixel level rather than in the latent space [35]; (3) the advantages of multi-stage conditioning over conditioning applied only at the final stage; and (4) the benefits of encoder-based conditioning relative to conditioning on the U-Net decoder. The quantitative DSSIM map estimation outcomes, as summarized in Table 5, substantiate the validity and soundness of our architectural choices.

Table 7. Evaluation of model generality. Integrating DiffusionFF as an auxiliary module consistently enhances the performance of existing forgery detectors, demonstrating its effectiveness as a plug-and-play improvement for face forgery detection models.

Method	Params	Test Set AUC (%) $\uparrow$			
		CDF2	DFDC	DFDCP	FFIW
EfficientNet-B4	19M	93.18	72.42	86.15	84.83
+ DiffusionFF	32M	95.54	82.19	89.03	86.37
Swin-B	88M	95.59	82.81	89.74	85.38
+ DiffusionFF	101M	96.93	84.54	90.78	87.01
ConvNeXt-B	89M	96.08	84.26	90.20	87.67
+ DiffusionFF	102M	<b>97.24</b>	<b>85.05</b>	<b>92.56</b>	<b>88.56</b>

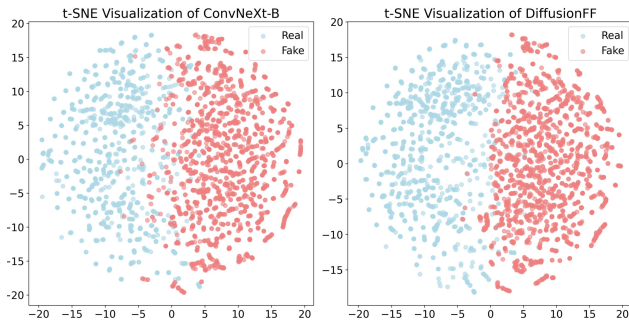


Figure 6. t-SNE visualizations of feature representations extracted by ConvNeXt and DiffusionFF on the CDF2 dataset. Compared to ConvNeXt, DiffusionFF yields more distinct and well-separated clusters, demonstrating its superior discriminative capability.

### 4.3.2. Ablation Study on the Fusion Module

To assess the effectiveness of the gating mechanism for feature fusion, we perform comparative experiments against several alternative strategies, including addition, Hadamard product, concatenation, and cross-attention [48]. As shown in Table 6, the cross-dataset detection results demonstrate the superior ability of the gating mechanism to seamlessly integrate artifact-aware and high-level semantic features.

### 4.3.3. Evaluation of Model Generality

We evaluate the generality of the DiffusionFF framework by examining its ability to enhance the detection performance of various forgery detectors. Our study considers two CNN-based models, EfficientNet [43] and ConvNeXt [26], as well as the Transformer-based Swin model [25]. For each detector, we compare its baseline performance against its performance when augmented with DiffusionFF, which provides additional artifact localization maps serving as visual explanations. The Vision Transformer (ViT) [9] is excluded because its single-scale feature representation is incompatible with DiffusionFF’s multi-scale conditioning

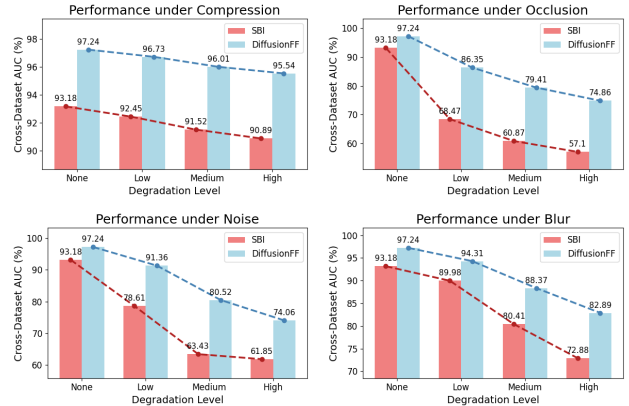


Figure 7. Evaluation of model robustness under various degradation conditions. DiffusionFF shows smaller performance declines than SBI [38] across all degradation types and severity levels.

mechanism. As shown in Table 7, all detectors exhibit consistent and substantial gains in cross-dataset detection performance when combined with DiffusionFF. Furthermore, t-SNE visualizations [47] in Figure 6 illustrate that DiffusionFF enables a clearer separation between real and fake samples than using the detector alone. These results confirm that integrating DiffusionFF as an auxiliary module significantly improves the performance of existing detectors, demonstrating its effectiveness as an explainable and plug-and-play enhancement for forgery detection models.

## 4.4. Evaluation of Model Robustness

We evaluate our model’s robustness across four real-world degradations, each applied at three severity levels: JPEG compression (quality factors of 95, 85, and 75), random occlusion (masking 2%, 5%, and 10% of pixels), Gaussian noise (standard deviations of 0.01, 0.05, and 0.1), and Gaussian blur (kernel/sigma values of 5/1, 7/2, and 9/3). As shown in Figure 7, the cross-dataset assessment results on the CDF2 dataset demonstrate that DiffusionFF consistently outperforms SBI [38] across all degradation conditions.

## 5. Conclusion

We propose DiffusionFF, a novel framework that simultaneously addresses the dual challenges of face forgery detection and fine-grained artifact localization. DiffusionFF introduces an innovative use of denoising diffusion models to estimate detailed DSSIM maps, enabling precise localization of fine-grained forgery clues and substantially improving detection capability. Extensive experiments demonstrate that our method not only achieves SOTA detection performance but also surpasses existing artifact localization approaches in revealing manipulation traces, underscoring its superior effectiveness, reliability, and explainability.

## References

- [1] Weiming Bai, Yufan Liu, Zhipeng Zhang, Bing Li, and Weiming Hu. Aunet: Learning relations between action units for face forgery detection. In *Proceedings of the IEEE/CVF Conference on Computer Vision and Pattern Recognition (CVPR)*, pages 24709–24719, 2023. 5, 6
- [2] Alexander Buslaev, Vladimir I Iglovikov, Eugene Khvedchenya, Alex Parinov, Mikhail Druzhinin, and Alexandr A Kalinin. Albumentations: fast and flexible image augmentations. *Information*, 11(2):125, 2020. 1
- [3] Shen Chen, Taiping Yao, Yang Chen, Shouhong Ding, Jilin Li, and Rongrong Ji. Local relation learning for face forgery detection. In *Proceedings of the AAAI conference on artificial intelligence (AAAI)*, pages 1081–1088, 2021. 1, 2, 5, 6
- [4] Shen Chen, Taiping Yao, Hong Liu, Xiaoshuai Sun, Shouhong Ding, Rongrong Ji, et al. Diffusionfake: Enhancing generalization in deepfake detection via guided stable diffusion. *Advances in Neural Information Processing Systems (NeurIPS)*, 37:101474–101497, 2024. 3
- [5] Xinjie Cui, Yuezun Li, Ao Luo, Jiaran Zhou, and Junyu Dong. Forensics adapter: Adapting clip for generalizable face forgery detection. In *Proceedings of the Computer Vision and Pattern Recognition Conference (CVPR)*, pages 19207–19217, 2025. 2
- [6] Jiankang Deng, Jia Guo, Evangelos Ververas, Irene Kotisia, and Stefanos Zafeiriou. Retinaface: Single-shot multi-level face localisation in the wild. In *Proceedings of the IEEE/CVF Conference on Computer Vision and Pattern Recognition (CVPR)*, 2020. 1
- [7] Brian Dolhansky, Russ Howes, Ben Pflaum, Nicole Baram, and Cristian Canton Ferrer. The deepfake detection challenge (dfdc) preview dataset. *arXiv preprint arXiv:1910.08854*, 2019. 5, 1
- [8] Brian Dolhansky, Joanna Bitton, Ben Pflaum, Jikuo Lu, Russ Howes, Menglin Wang, and Cristian Canton Ferrer. The deepfake detection challenge (dfdc) dataset. *arXiv preprint arXiv:2006.07397*, 2020. 5, 1
- [9] Alexey Dosovitskiy, Lucas Beyer, Alexander Kolesnikov, Dirk Weissenborn, Xiaohua Zhai, Thomas Unterthiner, Mostafa Dehghani, Matthias Minderer, Georg Heigold, Sylvain Gelly, Jakob Uszkoreit, and Neil Houlsby. An image is worth 16x16 words: Transformers for image recognition at scale. In *International Conference on Learning Representation (ICLR)*, 2021. 8
- [10] Xinghe Fu, Zhiyuan Yan, Taiping Yao, Shen Chen, and Xi Li. Exploring unbiased deepfake detection via token-level shuffling and mixing. In *Proceedings of the AAAI Conference on Artificial Intelligence (AAAI)*, pages 3040–3048, 2025. 5
- [11] Yue-Hua Han, Tai-Ming Huang, Kai-Lung Hua, and Jun-Cheng Chen. Towards more general video-based deepfake detection through facial component guided adaptation for foundation model. In *Proceedings of the IEEE/CVF Conference on Computer Vision and Pattern Recognition (CVPR)*, pages 22995–23005, 2025. 5
- [12] Peisong He, Haoliang Li, and Hongxia Wang. Detection of fake images via the ensemble of deep representations from multi color spaces. In *2019 IEEE International Conference on Image Processing (ICIP)*, pages 2299–2303, 2019. 2
- [13] Martin Heusel, Hubert Ramsauer, Thomas Unterthiner, Bernhard Nessler, and Sepp Hochreiter. Gans trained by a two time-scale update rule converge to a local nash equilibrium. *Advances in neural information processing systems (NeurIPS)*, 30, 2017. 6
- [14] Jonathan Ho, Ajay Jain, and Pieter Abbeel. Denoising diffusion probabilistic models. *Advances in neural information processing systems (NeurIPS)*, 33:6840–6851, 2020. 2, 3
- [15] Gee-Sern Hsu, Chun-Hung Tsai, and Hung-Yi Wu. Dual-generator face reenactment. In *Proceedings of the IEEE/CVF Conference on Computer Vision and Pattern Recognition (CVPR)*, pages 642–650, 2022. 1
- [16] Juan Hu, Xin Liao, Difei Gao, Satoshi Tsutsui, Qian Wang, Zheng Qin, and Mike Zheng Shou. Delocate: detection and localization for deepfake videos with randomly-located tampered traces. In *Proceedings of the Thirty-Third International Joint Conference on Artificial Intelligence (IJCAI)*, 2024. 1, 2, 5
- [17] Baojin Huang, Zhongyuan Wang, Jifan Yang, Jiaxin Ai, Qin Zou, Qian Wang, and Dengpan Ye. Implicit identity driven deepfake face swapping detection. In *Proceedings of the IEEE/CVF Conference on Computer Vision and Pattern Recognition (CVPR)*, pages 4490–4499, 2023. 2
- [18] Gengyun Jia, Meisong Zheng, Chuanrui Hu, Xin Ma, Yuting Xu, Luoqi Liu, Yafeng Deng, and Ran He. Inconsistency-aware wavelet dual-branch network for face forgery detection. *IEEE Transactions on Biometrics, Behavior, and Identity Science*, 3(3):308–319, 2021. 2
- [19] Davis E King. Dlib-ml: A machine learning toolkit. *The Journal of Machine Learning Research*, 10:1755–1758, 2009. 1
- [20] Chenqi Kong, Baoliang Chen, Haoliang Li, Shiqi Wang, Anderson Rocha, and Sam Kwong. Detect and locate: Exposing face manipulation by semantic-and noise-level telltales. *IEEE Transactions on Information Forensics and Security*, 17:1741–1756, 2022. 1, 2
- [21] Mohammad Rami Koujan, Michail Christos Doukas, Anastasios Roussos, and Stefanos Zafeiriou. Head2head: Video-based neural head synthesis. In *2020 15th IEEE International Conference on Automatic Face and Gesture Recognition (FG 2020)*, pages 16–23, 2020. 1
- [22] Nicolas Larue, Ngoc-Son Vu, Vitomir Struc, Peter Peer, and Vassilis Christophides. Seeable: Soft discrepancies and bounded contrastive learning for exposing deepfakes. In *Proceedings of the IEEE/CVF International Conference on Computer Vision (ICCV)*, pages 21011–21021, 2023. 5
- [23] Jiaming Li, Hongtao Xie, Lingyun Yu, and Yongdong Zhang. Wavelet-enhanced weakly supervised local feature learning for face forgery detection. In *Proceedings of the 30th ACM International Conference on Multimedia (ACM MM)*, page 1299–1308, 2022. 2
- [24] Yuezun Li, Xin Yang, Pu Sun, Honggang Qi, and Siwei Lyu. Celeb-df: A large-scale challenging dataset for deepfake forensics. In *Proceedings of the IEEE/CVF Conference*

- on *Computer Vision and Pattern Recognition (CVPR)*, 2020. 5, 2
- [25] Ze Liu, Yutong Lin, Yue Cao, Han Hu, Yixuan Wei, Zheng Zhang, Stephen Lin, and Baining Guo. Swin transformer: Hierarchical vision transformer using shifted windows. In *Proceedings of the IEEE/CVF International Conference on Computer Vision (ICCV)*, pages 10012–10022, 2021. 8
- [26] Zhuang Liu, Hanzi Mao, Chao-Yuan Wu, Christoph Feichtenhofer, Trevor Darrell, and Saining Xie. A convnet for the 2020s. In *Proceedings of the IEEE/CVF Conference on Computer Vision and Pattern Recognition (CVPR)*, pages 11976–11986, 2022. 6, 8, 1
- [27] Ilya Loshchilov and Frank Hutter. Decoupled weight decay regularization. *arXiv preprint arXiv:1711.05101*, 2017. 6, 1
- [28] Scott McCloskey and Michael Albright. Detecting gan-generated imagery using saturation cues. In *2019 IEEE International Conference on Image Processing (ICIP)*, pages 4584–4588, 2019. 2
- [29] Changtao Miao, Zichang Tan, Qi Chu, Huan Liu, Honggang Hu, and Nenghai Yu. F2trans: High-frequency fine-grained transformer for face forgery detection. *IEEE Transactions on Information Forensics and Security*, 18:1039–1051, 2023. 5
- [30] Dat Nguyen, Nesryne Mejri, Inder Pal Singh, Polina Kulshova, Marcella Astrid, Anis Kacem, Enjie Ghorbel, and Djamilia Aouada. Laa-net: Localized artifact attention network for quality-agnostic and generalizable deepfake detection. In *Proceedings of the IEEE/CVF Conference on Computer Vision and Pattern Recognition (CVPR)*, pages 17395–17405, 2024. 5
- [31] Yuval Nirkin, Yosi Keller, and Tal Hassner. Fsgan: Subject agnostic face swapping and reenactment. In *Proceedings of the IEEE/CVF International Conference on Computer Vision (ICCV)*, pages 7184–7193, 2019. 1
- [32] Gan Pei, Jiangning Zhang, Menghan Hu, Zhenyu Zhang, Chengjie Wang, Yunsheng Wu, Guangtao Zhai, Jian Yang, Chunhua Shen, and Dacheng Tao. Deepfake generation and detection: A benchmark and survey. *arXiv preprint arXiv:2403.17881*, 2024. 2
- [33] Siran Peng, Tianshuo Zhang, Li Gao, Xiangyu Zhu, Haoyuan Zhang, Kai Pang, and Zhen Lei. Wmamba: Wavelet-based mamba for face forgery detection. *arXiv preprint arXiv:2501.09617*, 2025. 2
- [34] Yuyang Qian, Guojun Yin, Lu Sheng, Zixuan Chen, and Jing Shao. Thinking in frequency: Face forgery detection by mining frequency-aware clues. In *Proceedings of The 16th European conference on computer vision (ECCV)*, pages 86–103. Springer, 2020. 2
- [35] Robin Rombach, Andreas Blattmann, Dominik Lorenz, Patrick Esser, and Björn Ommer. High-resolution image synthesis with latent diffusion models. In *Proceedings of the IEEE/CVF conference on computer vision and pattern recognition (CVPR)*, pages 10684–10695, 2022. 3, 7
- [36] Olaf Ronneberger, Philipp Fischer, and Thomas Brox. U-net: Convolutional networks for biomedical image segmentation. In *International Conference on Medical Image Computing and Computer Assisted Intervention (MICCAI)*, pages 234–241. Springer, 2015. 2, 4, 6, 1
- [37] Andreas Rossler, Davide Cozzolino, Luisa Verdoliva, Christian Riess, Justus Thies, and Matthias Niessner. Faceforensics++: Learning to detect manipulated facial images. In *Proceedings of the IEEE/CVF International Conference on Computer Vision (ICCV)*, 2019. 1, 5
- [38] Kaede Shiohara and Toshihiko Yamasaki. Detecting deepfakes with self-blended images. In *Proceedings of the IEEE/CVF Conference on Computer Vision and Pattern Recognition (CVPR)*, pages 18720–18729, 2022. 5, 6, 8, 1
- [39] Kaede Shiohara, Xingchao Yang, and Takafumi Take-tomi. Blendface: Re-designing identity encoders for face-swapping. In *Proceedings of the IEEE/CVF International Conference on Computer Vision (ICCV)*, pages 7634–7644, 2023. 1
- [40] Jiaming Song, Chenlin Meng, and Stefano Ermon. Denoising diffusion implicit models. *arXiv preprint arXiv:2010.02502*, 2020. 2
- [41] Ke Sun, Taiping Yao, Shen Chen, Shouhong Ding, Jilin Li, and Rongrong Ji. Dual contrastive learning for general face forgery detection. In *Proceedings of the AAAI Conference on Artificial Intelligence (AAAI)*, pages 2316–2324, 2022. 5
- [42] Chuangchuan Tan, Yao Zhao, Shikui Wei, Guanghua Gu, Ping Liu, and Yunchao Wei. Frequency-aware deepfake detection: Improving generalizability through frequency space domain learning. In *Proceedings of the AAAI Conference on Artificial Intelligence (AAAI)*, pages 5052–5060, 2024. 2
- [43] Mingxing Tan and Quoc Le. Efficientnet: Rethinking model scaling for convolutional neural networks. In *Proceedings of the 36th International Conference on Machine Learning (ICML)*, pages 6105–6114, 2019. 8
- [44] Justus Thies, Michael Zollhofer, Marc Stamminger, Christian Theobalt, and Matthias Niessner. Face2face: Real-time face capture and reenactment of rgb videos. In *Proceedings of the IEEE Conference on Computer Vision and Pattern Recognition (CVPR)*, 2016. 5
- [45] Justus Thies, Michael Zollhöfer, and Matthias Nießner. Deferred neural rendering: Image synthesis using neural textures. *ACM Transactions on Graphics*, 38(4):1–12, 2019. 5
- [46] Jiahe Tian, Cai Yu, Xi Wang, Peng Chen, Zihao Xiao, Jiao Dai, Jizhong Han, and Yesheng Chai. Real appearance modeling for more general deepfake detection. In *Proceedings of The 18th European Conference on Computer Vision (ECCV)*, pages 402–419, 2024. 5, 6
- [47] Laurens Van der Maaten and Geoffrey Hinton. Visualizing data using t-sne. *Journal of machine learning research*, 9 (11), 2008. 8
- [48] Ashish Vaswani, Noam Shazeer, Niki Parmar, Jakob Uszkoreit, Llion Jones, Aidan N Gomez, Lukasz Kaiser, and Illia Polosukhin. Attention is all you need. In *Advances in Neural Information Processing Systems (NeurIPS)*, 2017. 8
- [49] Jian Wang, Yunlian Sun, and Jinhui Tang. Lisiam: Localization invariance siamese network for deepfake detection. *IEEE Transactions on Information Forensics and Security*, 17:2425–2436, 2022. 1, 2, 5, 6
- [50] Zhou Wang, A.C. Bovik, H.R. Sheikh, and E.P. Simoncelli. Image quality assessment: from error visibility to structural similarity. *IEEE Transactions on Image Processing*, 13(4): 600–612, 2004. 1, 6

- [51] Zhiyuan Yan, Yong Zhang, Yanbo Fan, and Baoyuan Wu. Ucf: Uncovering common features for generalizable deepfake detection. In *Proceedings of the IEEE/CVF International Conference on Computer Vision (ICCV)*, pages 22412–22423, 2023. 2
- [52] Zhiyuan Yan, Yuhao Luo, Siwei Lyu, Qingshan Liu, and Baoyuan Wu. Transcending forgery specificity with latent space augmentation for generalizable deepfake detection. In *Proceedings of the IEEE/CVF Conference on Computer Vision and Pattern Recognition (CVPR)*, pages 8984–8994, 2024. 2
- [53] Zhiyuan Yan, Jiangming Wang, Peng Jin, Ke-Yue Zhang, Chengchun Liu, Shen Chen, Taiping Yao, Shouhong Ding, Baoyuan Wu, and Li Yuan. Orthogonal subspace decomposition for generalizable ai-generated image detection. *arXiv preprint arXiv:2411.15633*, 2025. 5
- [54] Ziming Yang, Jian Liang, Yuting Xu, Xiao-Yu Zhang, and Ran He. Masked relation learning for deepfake detection. *IEEE Transactions on Information Forensics and Security*, 18:1696–1708, 2023. 2
- [55] Peipeng Yu, Jianwei Fei, Zhihua Xia, Zhili Zhou, and Jian Weng. Improving generalization by commonality learning in face forgery detection. *IEEE Transactions on Information Forensics and Security*, 17:547–558, 2022. 2
- [56] Peipeng Yu, Jianwei Fei, Hui Gao, Xuan Feng, Zhihua Xia, and Chip Hong Chang. Unlocking the capabilities of vision-language models for generalizable and explainable deepfake detection. *arXiv e-prints*, pages arXiv–2503, 2025. 5
- [57] Zeqin Yu, Jiangqun Ni, Yuzhen Lin, Haoyi Deng, and Bin Li. Diffforensics: Leveraging diffusion prior to image forgery detection and localization. In *Proceedings of the IEEE/CVF Conference on Computer Vision and Pattern Recognition (CVPR)*, pages 12765–12774, 2024. 3
- [58] Daichi Zhang, Zihao Xiao, Shikun Li, Fanzhao Lin, Jianmin Li, and Shiming Ge. Learning natural consistency representation for face forgery video detection. In *Proceedings of The 18th European Conference on Computer Vision (ECCV)*, pages 407–424. Springer, 2024. 2
- [59] Lvmin Zhang, Anyi Rao, and Maneesh Agrawala. Adding conditional control to text-to-image diffusion models. In *Proceedings of the IEEE/CVF international conference on computer vision (CVPR)*, pages 3836–3847, 2023. 2
- [60] Richard Zhang, Phillip Isola, Alexei A. Efros, Eli Shechtman, and Oliver Wang. The unreasonable effectiveness of deep features as a perceptual metric. In *Proceedings of the IEEE Conference on Computer Vision and Pattern Recognition (CVPR)*, 2018. 6
- [61] Hanqing Zhao, Wenbo Zhou, Dongdong Chen, Tianyi Wei, Weiming Zhang, and Nenghai Yu. Multi-attentional deepfake detection. In *Proceedings of the IEEE/CVF Conference on Computer Vision and Pattern Recognition (CVPR)*, pages 2185–2194, 2021. 2
- [62] Hongjie Zhao, Beibei Liu, Yongjian Hu, Jicheng Li, and Chang-Tsun Li. Hybrid domain meta-learning network for face forgery detection and localization in deepfakes. In *2023 International Joint Conference on Neural Networks (IJCNN)*, pages 1–8. IEEE, 2023. 1, 2
- [63] Tianchen Zhao, Xiang Xu, Mingze Xu, Hui Ding, Yuanjun Xiong, and Wei Xia. Learning self-consistency for deepfake detection. In *Proceedings of the IEEE/CVF International Conference on Computer Vision (ICCV)*, pages 15023–15033, 2021. 2, 5, 6
- [64] Jiaran Zhou, Yuezun Li, Baoyuan Wu, Bin Li, Junyu Dong, et al. Freqblender: Enhancing deepfake detection by blending frequency knowledge. In *Advances in Neural Information Processing Systems (NeurIPS)*, pages 44965–44988, 2024. 5
- [65] Tianfei Zhou, Wenguan Wang, Zhiyuan Liang, and Jianbing Shen. Face forensics in the wild. In *Proceedings of the IEEE/CVF Conference on Computer Vision and Pattern Recognition (CVPR)*, pages 5778–5788, 2021. 5

# DiffusionFF: A Diffusion-based Framework for Joint Face Forgery Detection and Fine-Grained Artifact Localization

## Supplementary Material

### 6. Additional Implementation Details

#### 6.1. SBI

The SBI framework [38] synthesizes pseudo-fake facial images from real samples by simulating the deepfake generation process. It consists of two main components: the Source-Target Generator (STG) and the Mask Generator (MG). The STG applies a series of image transformations to create a pseudo-source and a pseudo-target image, while the MG produces a blending mask based on pre-detected facial landmarks, with augmentation to enhance diversity. The pseudo-source and pseudo-target images are then combined using the blending mask to generate a pseudo-fake facial image. In this study, we employ the SBI framework to augment the training data by integrating SBI-generated samples with those from the original FF++ dataset [37]. A key advantage of this approach is that the pseudo-fake images are perfectly aligned with their real counterparts, allowing for the precise computation of GT DSSIM maps.

#### 6.2. Preprocessing

During training, we extract 32 frames from each real video and 8 frames from each fake video to maintain a balanced ratio between positive and negative samples, as each real video corresponds to four manipulated ones. Additionally, we sample 8 frames from each real video to generate pseudo-fake samples using the SBI framework, which are incorporated into the training set to enhance data diversity. During testing, we uniformly sample 32 frames per video. Facial landmarks are extracted using Dlib’s 81-point predictor [19], which is utilized only during the training phase. For face detection, RetinaFace [6] is employed to obtain facial bounding boxes. During training, each detected face is cropped with a random margin ranging from 4% to 20%, while a fixed margin of 12.5% is applied during inference.

#### 6.3. Data Augmentation

The image processing toolbox introduced in [2] is employed for data augmentation. Within the STG module of the SBI framework, transformations including RGBShift, HueSaturationValue, RandomBrightnessContrast, Downscale, and Sharpen are applied to generate pseudo source and target images. During training, all samples are augmented using operations such as ImageCompression, RGBShift, HueSaturationValue, and RandomBrightnessContrast. These augmentations expose the model to a broader range of visual variations, thereby enhancing its generalization capability.

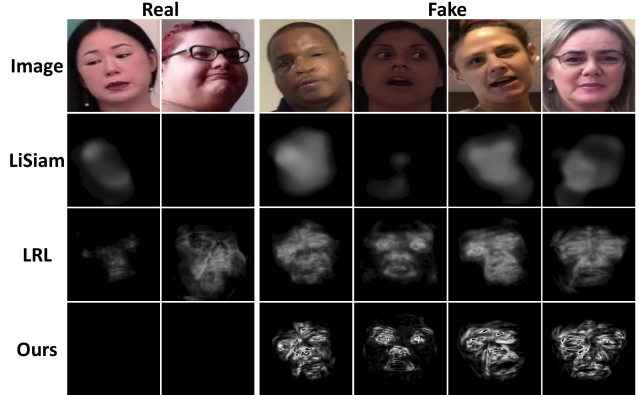


Figure 8. Qualitative DSSIM map estimation results on the DFDC dataset. Our DiffusionFF framework generates more fine-grained and detailed artifact localization maps than competing approaches. Note that GT DSSIM maps are unavailable for this dataset.

#### 6.4. Additional Details

The ConvNeXt-B detector [26] is trained on the FF++ dataset with SBI-based data augmentation. Training is conducted for 200 epochs using the AdamW optimizer [27], with a batch size of 64 and an initial learning rate of  $5 \times 10^{-5}$ . To promote stable convergence, a linear learning rate decay is applied starting from epoch 100. For the diffusion model, we employ a standard seven-stage U-Net architecture [36] with channel dimensions configured as [64, 64, 128, 256, 128, 64, 64]. For the noise schedule, the per-step variances  $\{\beta_t\}_{t=1}^T$  increase linearly from 0.02 to 0.4. The GT DSSIM maps are generated using a local square window of size  $7 \times 7$ . For frames containing multiple detected faces, the classification model is applied to each face, and the maximum score is taken as the frame-level confidence.

### 7. Additional Experiments

#### 7.1. Additional Qualitative Evaluation

In the DFDC [8] and DFDCP [7] datasets, the real and fake video pairs are not spatially aligned, which prevents the generation of GT DSSIM maps for quantitative evaluation. To assess the generalization capability of our DiffusionFF framework under this situation, we provide a qualitative comparison against existing DSSIM-based approaches on the DFDC dataset, as shown in Figure 8. Although GT DSSIM maps are unavailable, the visual results clearly in-

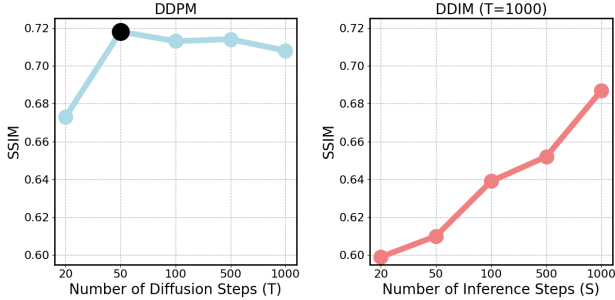


Figure 9. Ablation study on the training and inference settings of the diffusion model. The DDPM framework with  $T = 50$  delivers the best performance, marked by the black dot in the left figure.

dicating that DiffusionFF produces the most fine-grained and detailed outcomes, underscoring its superior effectiveness in generating high-quality artifact localization maps.

## 7.2. Additional Ablation Studies

### 7.2.1. Training & Inference of the Diffusion Model

In this study, we employ the standard DDPM framework [14], where the number of inference steps is set equal to the number of training diffusion steps ( $T$ ). We begin by examining how varying  $T$  affects performance. The quantitative results shown on the left of Figure 9 indicate that our model achieves optimal performance at  $T = 50$ . This outcome contrasts with the common expectation that larger  $T$  values generally lead to better generation quality. We hypothesize that this discrepancy arises because our conditional DSSIM estimation task differs fundamentally from traditional RGB image generation, thereby shifting the optimal hyper-parameter landscape. To further validate our framework choice, we also evaluate the Denoising Diffusion Implicit Model (DDIM) framework [40], which enables faster inference by skipping diffusion steps. In this experiment, we use a model trained with  $T = 1000$  and perform inference using  $S$  sampling steps. As shown on the right of Figure 9, while DDIM performance improves with increasing  $S$ , it consistently underperforms the DDPM  $T = 1000$  baseline, let alone the superior DDPM  $T = 50$  setup. Collectively, these findings firmly validate our choice to use the DDPM framework with a small timestep of  $T = 50$ .

### 7.2.2. Denoising Seeds

We evaluate the impact of random seed variation on DSSIM map estimation performance. As illustrated in Figure 10, our DiffusionFF framework consistently generates stable and reliable artifact localization maps across different seeds.

### 7.2.3. Two-Stage Training Strategy

We compare our two-stage training strategy against a single-stage baseline that jointly optimizes DSSIM map es-

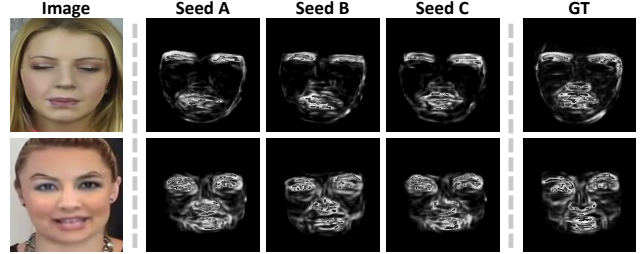


Figure 10. Ablation study on denoising seeds. Our method consistently generates stable localization maps across different seeds.

Method	Test Set AUC (%) $\uparrow$			
	CDF2	DFDC	DFDCP	FFIW
Single-Stage	95.47	83.54	90.27	87.69
Two-Stage	<b>97.24</b>	<b>85.05</b>	<b>92.56</b>	<b>88.56</b>

Table 8. Ablation study on the two-stage training strategy.

timization and binary classification. As shown in Table 8, our approach yields significantly better results, demonstrating the effectiveness of training these two tasks separately.

## 8. Discussions

In this section, we discuss three critical questions: (1) Can GT DSSIM maps serve as inputs to the artifact feature extractor during our second training stage? (2) Is the ControlNet framework [59] capable of estimating DSSIM maps? and (3) What causes the joint training of the forgery detector and diffusion model from scratch to fail? Additionally, we summarize the strengths and limitations of our work.

### 8.1. GT DSSIM Maps As Inputs During Training

In Figure 2 of the main text, we demonstrate a clear positive correlation: the higher the quality of the DSSIM maps integrated into the detection network, the greater the resulting performance gains. This observation naturally leads to the question: what if GT DSSIM maps were used as inputs to the artifact feature extractor during our second training stage? To explore this, we conduct an experiment using GT DSSIM maps and obtain a 96.72% AUC on the CDF2 dataset [24], which is lower than the 97.24% AUC achieved with diffusion-estimated maps. This performance drop is primarily due to a mismatch in value distributions: GT DSSIM maps (e.g., all zeros for real samples) differ significantly from those estimated by the diffusion model. As a result, a model trained with GT DSSIM maps struggles to generalize when faced with diffusion-estimated inputs during inference, ultimately leading to degraded performance.

## 8.2. ControlNet for DSSIM Map Estimation

ControlNet is a widely adopted framework for conditional image generation that integrates an auxiliary conditioning network to guide a pretrained, frozen Stable Diffusion model [35]. **In our study, we attempted to train a ControlNet to estimate DSSIM maps but encountered training collapse, where the network produces identical, content-irrelevant outputs regardless of input variation.** We attribute this failure to a fundamental domain mismatch: the pretrained Stable Diffusion model, optimized for natural RGB image synthesis, struggles to adapt to single-channel, grayscale DSSIM maps due to its strong prior knowledge. To overcome this limitation, we propose an inverted strategy that contrasts with the conventional ControlNet paradigm. Instead of training a new conditioning network, we employ a pretrained forgery detector as a fixed conditioning model, leveraging its capacity to capture forgery-related features. By freezing the conditioning network and training the diffusion model instead, we shift the learning focus to the generative model itself. This reversal allows the diffusion model to effectively utilize the detector’s specialized features, enabling precise and stable estimation of DSSIM maps.

## 8.3. Training Detector and Diffusion From Scratch

As noted in Section 3.2.2, jointly training the forgery detector and diffusion model from scratch leads to training collapse. Here, we analyze this failure in detail. **During training, the model converges to a trivial solution: producing entirely black images regardless of input.** This collapse arises because the GT DSSIM maps for real images are uniformly black. Consequently, predicting black results in zero loss for real samples, allowing the model to minimize training loss without learning the more complex task of detecting and localizing artifacts in fake images. This behavior highlights that the DSSIM estimation task intrinsically depends on forgery-related features. Without explicit guidance from these features, the diffusion model fails to learn the distinction between real and fake faces. To address this issue, we employ a pretrained forgery detector to extract forgery-specific features that guide the diffusion model in generating fine-grained artifact localization maps.

## 8.4. Strengths & Limitations

### 8.4.1. Strengths

The proposed DiffusionFF framework exhibits three key advantages. First, it enables precise localization of fine-grained forgery clues, thereby enhancing model explainability and fostering greater user trust. Second, by integrating the generated artifact localization maps into the detection pipeline, DiffusionFF significantly improves overall detection performance. Third, owing to its strong generality, DiffusionFF can serve as an explainable, plug-and-play enhancement for existing face forgery detection models.

### 8.4.2. Limitations

Despite its many advantages, the DiffusionFF framework also presents two limitations. First, the inference process of the diffusion model is time-consuming. Second, our method is not designed for entirely synthesized images.